Mito-LND and (E)-Akt inhibitor-IV: novel compounds inducing endoplasmic reticulum stress and ROS accumulation against hepatocellular carcinoma

Siqi Liao[1†], Qingliang Wang[2†], Siyuan Chen[1], Qixuan Huang[3], Li Zhou[1], Hongtao Liu[1], Song He[1*] and Zhihang Zhou[1*]

Abstract

Background Hepatocellular carcinoma (HCC) is one of the leading causes of cancer-related mortality. Although multi-kinase inhibitors can prolong the overall survival of late-stage HCC patients, the emergence of drug resistance diminishes these benefits, ultimately resulting in treatment failure. Therefore, there is an urgent need for novel and effective drugs to impede the progression of liver cancer.

Methods This study employed a concentration gradient increment method to establish acquired sorafenib or regorafenib-resistant SNU-449 cells. Cell viability was assessed using the cell counting kit-8 assay. A library of 793 bioactive small molecules related to metabolism screened compounds targeting both parental and drug-resistant cells. The screened compounds will be added to both the HCC parental cells and the drug-resistant cells, followed by a comprehensive assessment. Intracellular adenosine triphosphate (ATP) levels were quantified using kits. Flow cytometry was applied to assess cell apoptosis and reactive oxygen species (ROS). Real-time quantitative PCR studied relative gene expression, and western blot analysis assessed protein expression changes in HCC parental and drug-resistant cells. A xenograft model in *vivo* evaluated Mito-LND and (E)-Akt inhibitor-IV effects on liver tumors, with hematoxylin and eosin staining for tissue structure and immunohistochemistry staining for endoplasmic reticulum stress protein expression.

Results From the compound library, we screened out two novel compounds, Mito-LND and (E)-Akt inhibitor-IV, which could potently kill both parental cells and drug-resistant cells. Mito-LND could significantly suppress proliferation and induce apoptosis in HCC parental and drug-resistant cells by upregulating glycolytic intermediates and downregulating those of the tricarboxylic acid (TCA) cycle, thereby decreasing ATP production and increasing ROS. (E)-Akt inhibitor-IV achieved comparable results by reducing glycolytic intermediates, increasing TCA cycle

---

†Siqi Liao and Qingliang Wang contributed equally to this work.

*Correspondence:
Song He
hedoctor65@cqmu.edu.cn
Zhihang Zhou
zhouzhihang@cqmu.edu.cn

Full list of author information is available at the end of the article

intermediates, and decreasing ATP synthesis and ROS levels. Both compounds trigger apoptosis in HCC cells through the interplay of the AMPK/MAPK pathway and the endoplasmic reticulum stress response. In *vivo* assays also showed that these two compounds could significantly inhibit the growth of HCC cells and induce endoplasmic reticulum stress.

Conclusion Through high throughput screening, we identified that Mito-LND and (E)-Akt inhibitor-IV are two novel compounds against both parental and drug-resistant HCC cells, which could offer new strategies for HCC patients.

Keywords Hepatocellular carcinoma, Mito-LND, (E)-Akt inhibitor-IV, Drug-resistance, Mitochondria

Background

Hepatocellular carcinoma (HCC) constitutes 70-90% of primary liver cancers, making it the sixth most prevalent cancer and the third leading cause of cancer-related fatalities globally [1]. Currently, curative treatments for early-stage HCC patients include surgical resection, liver transplantation, and local ablation. However, most HCC patients are diagnosed at advanced stages, limiting treatment options to methods like transarterial chemoembolization and systemic therapies to extend survival [2]. Although multi-kinase inhibitors, like sorafenib, lenvatinib, and regorafenib, can prolong overall survival of advanced HCC patients, the evolution of HCC diminishes the efficacy and eventually leads to treatment failure [3]. Therefore, new and effective drugs that retardate cancer progression are urgently needed.

Metabolic reprogramming is one of the hallmarks of cancer [4], providing treatment vulnerabilities. Cancer cells undergo several metabolic adaptations to sustain continuous proliferation and metastasis. A century ago, Otto Warburg observed cancer cells using a lot of glucose to produce lactate, even with oxygen—a phenomenon known as aerobic glycolysis or the Warburg effect [5]. This increase in glycolysis leads to the production of glycolytic intermediates, such as pyruvate and lactate, which can be used as building blocks for the synthesis of new molecules, such as nucleotides, lipids, and amino acids, required for cell proliferation. These intermediates can also be converted into other metabolic intermediates through the tricarboxylic acid (TCA) cycle, which acts as an important hub for anabolism in cancer cells. By disrupting cancer cell metabolism or altering redox balance, it may be possible to inhibit tumor growth and improve patient outcomes [6]. Recent investigations have unveiled diverse metabolic reprogramming occurrences, such as an augmented requirement for electron acceptors, heightened dependence on shielding against oxidative stress, and escalated nitrogen demand [7]. The susceptibility resulting from metabolic reprogramming could present therapeutic prospects since cancer cells depend on particular metabolic pathways. For instance, in 1948, Farber and Diamond documented that aminopterin, an anti-folate medication, could bring about remission in pediatric acute lymphocytic leukemia [8].

Thereafter, numerous metabolic medications, such as the folate metabolism inhibitor methotrexate and various agents suppressing nucleotide synthesis, have received approval for clinical utilization [9]. Overall, these findings highlight the complex interplay between metabolism and cancer development and provide potential targets for therapeutic intervention.

Mitochondria are important bioenergetic and biosynthetic factories that are essential for normal cell function and human health. Mitochondria play a central and multifaceted role in the progression of malignant tumors, offering opportunities for targeted therapy in cancer [10]. Stimulating mitochondrial reactive oxygen species (ROS) generation to induce cancer cell death can enhance the efficacy of chemotherapy [11]. The complex I inhibitor metformin is a biguanide commonly used to treat diabetes and has anticancer activity in diabetic patients [12]. Succinate dehydrogenase (SDH)-deficient cells relying on extracellular pyruvate for Warburg-like bioenergetics and sustaining growth through pyruvate carboxylation, highlighting a metabolic vulnerability for potential SDH-associated malignancy treatment [13].

The compound library targeting cancer metabolism serves as a powerful tool for screening novel potent compounds against cancer. Imatinib, a tyrosine kinase inhibitor primarily used for treating chronic myeloid leukemia, was selected from the compound library [14]. Simultaneously, panitumumab was also discovered through library screening [15]. This highlights the compound library's effectiveness in targeting cancer metabolism, serving as a robust tool for screening novel compounds against cancer. Consequently, we conducted a study on mitochondria-targeted mito-lonidamine (Mito-LND) and (E)-Akt inhibitor-IV ((E)-AKTIV), identified from screening an anti-cancer metabolism compound library, to investigate their cytotoxic effects on both wild-type and drug-resistant HCC cells. Additionally, we delved into the potential underlying mechanisms of action.

Methods

Cell lines and cell culture

Human liver cancer cell lines Huh7, SK-Hep1, SNU-449 were obtained from the American Type Culture Collection (Manassas, VA, USA). All the cells were identified by

short-tandem-repeat profiling, and without mycoplasma contamination. Cells were cultured in Dulbecco's Modified Eagle Medium (DMEM) pH 7.4 (Gibco, Rockville, MD, USA). All culture media were supplemented with 10% fetal bovine serum (Natocor, SFBNTC, Natocor-Industria Biologica, Argentina), 100 units/mL penicillin, and 100 μg/mL streptomycin (HyClone). All cells were grown in a 37 °C humidified atmosphere containing 5% CO_2.

Drug resistant cultivation

The SNU-449 wild-type cells (SNU-449 WT) were subjected to a gradient increment induction method using the drugs (sorafenib/regorafenib), and resistant cultivation was carried out for a minimum of 8 months. After resistant cells and its parental cells (5000 cells per well) treated with 1 to 64 μM of regorafenib (HY-10331, MedChemExpress) and 1 to 32 μM of sorafenib (HY-10201, MedChemExpress) for 48 h, the cell viability was determined by cell counting kit-8 assay (CCK-8) (GlpBio, China). The resistance index (RI) was calculated according to the following formula: RI= (IC50 of the resistant cell line)/ (IC50 of the parental cell line).

High-throughput drug screening

In the screening of the anti-cancer metabolism compound library (HY-L083, MedChemExpress), 5000 SK-Hep1/Huh7/SNU-449/SNU-449 regorafenib-resistant cells (SNU-449 RR) were seeded per well in a 96-well plate. After cell attachment, each compound was added to the cells at a concentration of 10 μM. Following a 48-hour incubation period, absorbance was measured using CCK-8. The absorbance was measured at 450 nm by a microplate reader (Thermo varioskan lux). Cell viability (%) was calculated according to the formula: (experiment OD value-blank OD value)/ (control OD value-blank OD value) × 100%.

Protein extraction and Western blot analysis

SNU-449 WT, SNU-449 sorafenib-resistant cells (SNU-449 SR) and SNU-449 RR were treated with Mito-LND (HY-134832, MedChemExpress) or (E)-Akt inhibitor IV (HY-14971, MedChemExpress) at a concentration of 4 μM for 48 h. Subsequently, total protein was harvested. Cells were lysed using protein lysate (Beyotime, China) and the protein concentration of cell lysates was assessed by the bicinchoninic acid protein assay (Beyotime, China). 30 μg aliquots of proteins from whole cell lysates were separated by 8–12% sodium dodecyl sulfate-polyacrylamide gel electrophoresis and transferred to a PVDF membrane. Closure with NcmBlot blocking buffer for 30 min. The protein expression levels of AMPK (5832 S, Cell Signaling Technology), p-AMPK (2535 S, Cell Signaling Technology), AKT (9272 S, Cell Signaling

Technology), p-AKT (4060 S, Cell Signaling Technology), ERK (ET601-29, HUABIO), p-ERK (ET1610-13, HUABIO), P38 (66234-1-IG, Proteintech), p-P38 (YP0338, Immunoway), JNK (66210-1-IG, Proteintech), p-JNK (ET1601-28, HUABIO), mTOR (66888-1-IG, Proteintech), p-mTOR (67778-1-IG, Proteintech), IRE1 (27528-1-AP, Proteintech), p-IRE1 (YP1798, Abcam), XBP1S (24868-1-AP, Proteintech) and CHOP (15204-1-AP, Proteintech) were measured by specific antibodies with β-Tubulin (TA-10, ZSGB-BIO), vinculin (66305-1-IG, Proteintech), or β-actin (81115-1-RR, Proteintech) as the loading control.

Intracellular ATP assay

After overnight apposition of cells in 24-well plates, Mito-LND and (E) -AKTIV were added at 4 μ M concentrations. 1×10^5 cells per group after 48 h incubation, 100ul lysate was added, and cells were lysed on ice. Follow instructions according to the ATP extraction kit from Beyotime (Jiangsu, China).

Assessment of intracellular reactive oxygen species (ROS)

SNU-449 WT, SNU-449 SR and SNU-449 RR cells were seeded in 1×10^6 cells/well. After treatment with Mito-LND (4 μM) and (E)-AKTIV (4 μM) for 48 h, cells were collected and centrifuged at 1,000 rpm for 5 min. The DCFH-DA probe (Beyotime, China) was introduced and incubated at 37 °C for 20 min. Uninternalized probe was washed off twice with phosphate-buffered saline (PBS). Subsequently, the cells were transferred to flow tubes. Flow cytometry was employed to determine the percentage of ROS-positive cells, and the data were analyzed using FlowJo-V10 software.

Real-time quantitative PCR analysis

SNU-449 parental cells, along with the corresponding resistant cells SNU-449 SR and SNU-449 RR in the logarithmic growth phase, were treated with 0 or 4 μM Mito-LND or (E)-AKTIV for 48 h. Total RNA was isolated from cells by trizol reagent from Esscience (Shanghai, China) according to manufacturer's protocol. The isolated total RNA underwent reverse transcription to generate cDNA using a reverse transcription kit from SparkJade (Shandong, China). Subsequently, the CFX Opus real-time PCR system (Bio-Rad, USA) was employed to load the reverse transcription products obtained from the total RNA onto the Taq Man array for quantitative reverse transcription-polymerase chain reaction (RT-qPCR). The specificity of amplification was validated through melting curve analysis. Normalizing with the internal reference (B2M), the relative mRNA levels of genes were calculated using Ct values according to the formula: Ct value=$2^{\wedge}$-ΔCt [ΔCt=Ct target gene - Ct B2M]. The Ct value was utilized to determine the relative expression

level of gene mRNA. The entire experiment was replicated three times, and then the average was computed.

Primers used for RT-qPCR

Primer name	Primer sequence
XBP1_Forward	TGGCGGTATTGACTCTTCA
XBP1_Reverse	GGAACTGGGTCCTTCTGG
ATF4_Forward	GAGCAGCGAGGTGTTGG
ATF4_Reverse	CCCGCCTTAGCCTTGTC
B2M_Forward	GAGTGCTGTCTCCATGTTTG
B2M_Reverse	CTGCTCCCCACCTCTAAGT
GADD45A_Forward	GCCCGGAGATAGATGACTT
GADD45A_Reverse	TTTCCTTCCTGCATGGTT
ITPR1_Forward	AGGCTTCCTGCTCTGTTG
ITPR1_Reverse	CTATGACCACGCTGTCTCC
IRE1_Forward	ATCTCGGGGTGGTGCTC
IRE1_Reverse	CTGGGTCTTCGCTGCTCT
CHOP_Forward	CTTTCTCCTTCGGGACACT
CHOP_Reverse	GACCTCTGCTGGTTCTGG

Evaluation of cell apoptosis

Approximately 1×10^6 cells per well were collected, centrifuged at 1,000 rpm for 5 min at room temperature, resuspended in ice-cold PBS, centrifuged again at 1,000 rpm for 5 min, and then washed. Subsequent flow cytometry analysis was performed by a qualified instructor.

Transcriptome sequencing

Preparation of Normal Transcriptome Samples: SNU-449 WT cells were seeded in a 6-well plate at 75% confluency. After cell adhesion, 4 μM Mito-LND and (E)-AKTIV were added, with a control group designated as the untreated group. Each experimental condition was repeated three times. After 48 h, cells were lysed with 500 μL Takara trizol on ice and stored at -80 °C until analysis. The samples were sent to Oebiotech for further analysis (Shanghai, China).

Metabolome analysis

Metabolome Sample Preparation: SNU-449 WT cells were seeded in a 10 cm^2 dish at 75% confluency. After cell adhesion, 4 μM Mito-LND and (E)-AKTIV were added, with an untreated group as the control. Each experimental condition was repeated eight times. After 48 h, 1×10^7 cells from each group were collected and stored at -80 °C. The samples were sent to Oebiotech for further analysis (Shanghai, China) for gas chromatography-mass spectrometry (GC-MS) and liquid chromatography-mass spectrometry (LC-MS) analysis.

Drug synergism

Administer Mito-LND, (E)-AKTIV, sorafenib, and regorafenib at concentrations approximately half of their respective IC50 values to SNU-449 RR and SNU-449 SR cell lines for 48 h, observing their inhibitory effects on HCC proliferation. The combined effect of the drugs [16] is estimated using the following formula: $q=E_{AB}$ / [E_A + (1 - E_A) × E_B], where E_{AB} represents the inhibition rate when two drugs are used in combination, while E_A and E_B denote the individual inhibition rates of each drug alone. If q falls within the range of 0.85 to 1.15, it indicates an additive effect of the two drugs; if q > 1.15, it suggests a synergistic interaction between the drugs; conversely, if q < 0.85, it signifies antagonism when the drugs are used together.

Subcutaneous xenograft model

Four-week male athymic nude mice were obtained from Hunan Anshengmei Pharmaceutical Research Institute Co., Ltd. (Hunan, China), raised in the specific pathogen-free (SPF) -free environment. The animal experiments were approved by the Animal Ethics Committee of the Second Affiliated Hospital of Chongqing Medical University (Approval No: 2021−115) in accordance with the National Laboratory Animal Regulations of the China Science and Technology Commission. In brief, SK-hep1 cells (5×10^6) in 100 μL PBS were subcutaneously inoculated into the right flank of mice. The mice, randomized into three groups (n=6/group) – control, Mito-LND, (E)-AKTIV – received subcutaneous injections of Mito-LND and (E)-AKTIV at a dose of 100 μmol/kg, while the control group received daily saline injections. Tumor volume, calculated using the formula V=L×W^2/2 (where "W" is the longest transverse axis perpendicular to the longest axis, and "L" is the longest axis), was measured weekly. At the experiment's conclusion, tumors were harvested, and their weight and size were measured.

Orthotopic model

Four-week male NCG mice were obtained from GemPharmatech Company (Jiangsu, China), raised in the specific SPF -free environment. The animal experiments were approved by the Animal Ethics Committee of the Second Affiliated Hospital of Chongqing Medical University (Approval No: 2021−115) in accordance with the National Laboratory Animal Regulations of the China Science and Technology Commission. Mice were divided into three groups (Mito-LND, (E)-AKTIV, Control), with nine animals per group. One week later, NCG mice (5 weeks old) were anesthetized using isoflurane and placed in a supine position. Luciferase-expressing lentivirus was used to transduce SK-Hep1 (designated SK-Hep1-Luc) cells for imaging. 1×10^6 SK-Hep1-Luc cells suspended in 30 μL of growth factor-reduced matrigel (#356234,

Corning) were injected into the liver. Ten days post-injection, mice were gavaged daily for three consecutive weeks with Mito-LND, (E)-AKTIV, or vehicle control at a dose of 7.5µmol/kg. Tumor growth and metastasis were monitored utilizing an imaging system (AniView Kirin, Guangzhou, China) by intraperitoneally injecting D-Luciferin potassium salt (HY-12591B, MedChemExpress) into the mice, followed by imaging 10 min post-injection. Mice were euthanized on day 31, and livers and lungs were excised for further imaging. And perform HE staining on the heart, liver, spleen, lung, and kidney of the NCG mice.

Hematoxylin and eosin (H&E) and immunohistochemistry (IHC) staining

H&E and IHC analyses were performed on tissue sections obtained from formalin-fixed and paraffin-embedded tissue blocks of xenograft models. Immunohistochemical staining involved 4 µm FFPE unstained sections using antibodies targeting p-IRE1 (YP1798, Abcam) and CHOP (15204-1-AP, Proteintech). Deparaffinization of tissue sections was carried out using xylene, followed by rehydration in decreasing concentrations of ethanol. Antigen retrieval was conducted in a microwave oven for 30 min using sodium citrate buffer (pH=6.0). Endogenous peroxidase activity was suppressed with 3% H_2O_2 in methanol for 30 min, followed by overnight incubation with the primary antibody at 4 °C. After washed with PBS, slides were incubated with secondary antibody with streptavidin horseradish peroxidase for 20 min at 37 °C, then washing the slides with PBS. Diaminobenzidine stain for 5 min, and then hematoxylin counterstain for 5 min. Finally, sections were sealed with neutral resin and dried in a fume hood.

Statistical analysis

Statistical analyses were conducted using GraphPad Prism (version 9.5.1). Data with normal distributions underwent analysis through t-tests and ANOVA. A significance level of $P<0.05$ was applied to determine statistical significance.

Results

High-throughput analysis revealed that Mito-LND and (E)-AKTIV could potently kill both parental and drug-resistant HCC cells

Among the cells used in this study, SNU-449 cells exibited the lowest half maximal inhibitory concentration (IC50) to sorafenib and regorafenib (Fig.S1 A&B). Therefore, SNU-449 cell lines were employed to develop resistance to sorafenib and regorafenib. The initial assessment utilized the CCK-8 assay, revealing a significantly greater growth-suppressive effect of the two drugs in parental cells compared to their resistant counterparts

(Fig. 1A&B). IC50 value of SNU-449 wild type cells (also called SNU-449 WT) in sorafenib and regorafenib respectively were 1.98 µM and 7.954 µM. Nevertheless, IC50 of their resistant cells respectively increased to 6.518 µM and 58.59 µM (Fig. 1C&D). The resistance index of SNU-449 sorafenib-resistant cells (also called SNU-449 SR) and SNU-449 regorafenib-resistant cells (also called SNU-449 RR) was respectively 3.29 and 7.37.

After the establishment of resistant cell lines, 793 small-molecule compounds were screened against SK-Hep1 wild-type cells (SK-Hep1 WT) (Table S1). Thirty-two compounds demonstrated superior tumor-killing efficacy, defined as cell viability below 2%. Subsequently, these compounds were selected for evaluation against Huh7 wild-type cells (Huh7 WT) (Fig. 1E), SNU-449 WT (Fig. 1F), and SNU-449 RR (Fig. 1G). This led to the identification of two small-molecule compounds, Mito-LND and (E)-AKTIV, which could potently kill all the tested HCC cells (Fig. 1H). Interestingly, both Mito-LND (Fig. 1I) and (E)-AKTIV (Fig. 1J) were recognized to target mitochodria. All together, our high-throughput analysis revealed that Mito-LND and (E)-AKTIV were novel compounds to potently kill both parental and drug-resistant HCC cells.

Mito-LND and (E)-AKTIV restrained parental and drug-resistant HCC cells by increasing ROS level and imparing ATP synthesis

To investigate the anti-cancer effect of Mito-LND and (E)-AKTIV in inhibiting the growth of HCC cells, SNU-449 parental cells and drug-resistant cells were treated with these two compounds. Mito-LND and (E)-AKTIV significantly suppressed growth of the HCC parental cells or resistant cells. Mito-LND inhibited SNU-449 WT, SNU-449 SR, SNU-449 RR cell viability of 50% in the concentration of 2.757 µM, 5.941 µM, and 4.583 µM respectively (Fig. 2A). (E)-AKTIV inhibited SNU-449 WT, SNU-449 SR, SNU-449 RR cell viability of 50% in the concentration of 1.927 µM, 6.759 µM, and 4.9 µM respectively (Fig. 2B). Therefore, we employed a drug concentration of 4 µM for the pharmacological intervention. Both types of HCC resistant cells appear to be more resistant to these two drugs. Consistent with previous studies [17, 18], we found that Mito-LND promoted the elevation of ROS in HCC parental cells and two resistant cells (Fig. 2C-E). (E)-AKTIV is like AKTIV [19], with increased ROS compared to control (Fig. 2C-E). Glutathione (GSH) is one of the most important antioxidants in the cellular antioxidant system [20]. It has been shown that loss of GSH disrupts cellular redox homeostasis, leading to ROS accumulation and eventually triggering cell damage and even death [21].

We further analyzed the impact of Mito-LND and (E)-AKTIV on HCC metabolism by metabolomic analysis.
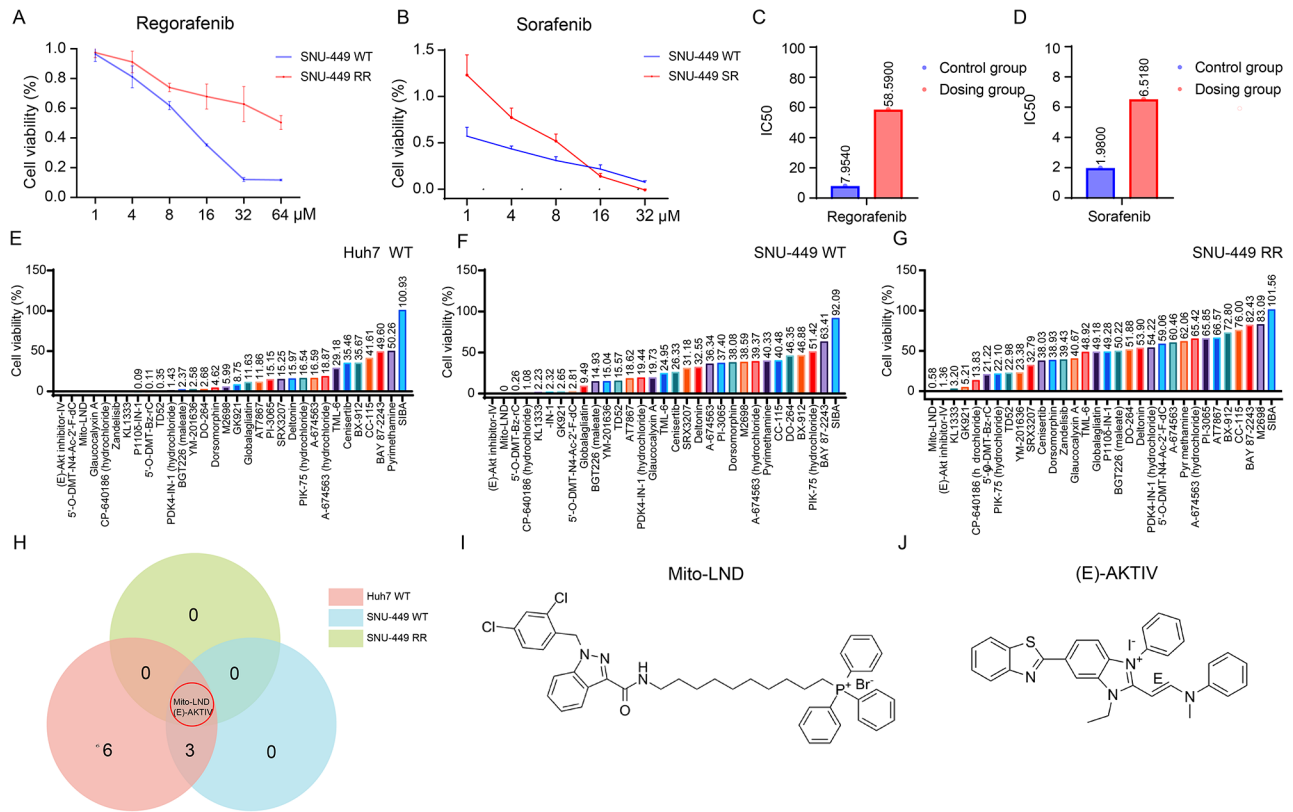
Fig. 1 New compounds to target HCC cells were found through drug-screening. **A&B** Treated with varying concentrations of sorafenib and regorafenib for 48 h, cell viability was assessed using the CCK-8 assay. **C&D** The IC50 values of the drugs in different cell types were calculated using GraphPad Prism. **E-G** Thirty-two drugs selected from the SK-Hep1 WT cell line were subjected to a CCK-8 assay at a concentration of 10 μM. Cell viability was then calculated for Huh7 WT, SNU-449 WT, and SNU-449 RR cell lines based on the experimental results. **H** The intersection was determined for the cell viability of the drugs in Huh7 WT, SNU-449 WT, and SNU-449 RR cell lines, where the viability was less than 2%. **I&J** The structural formulas of Mito-LND and (E)-AKTIV
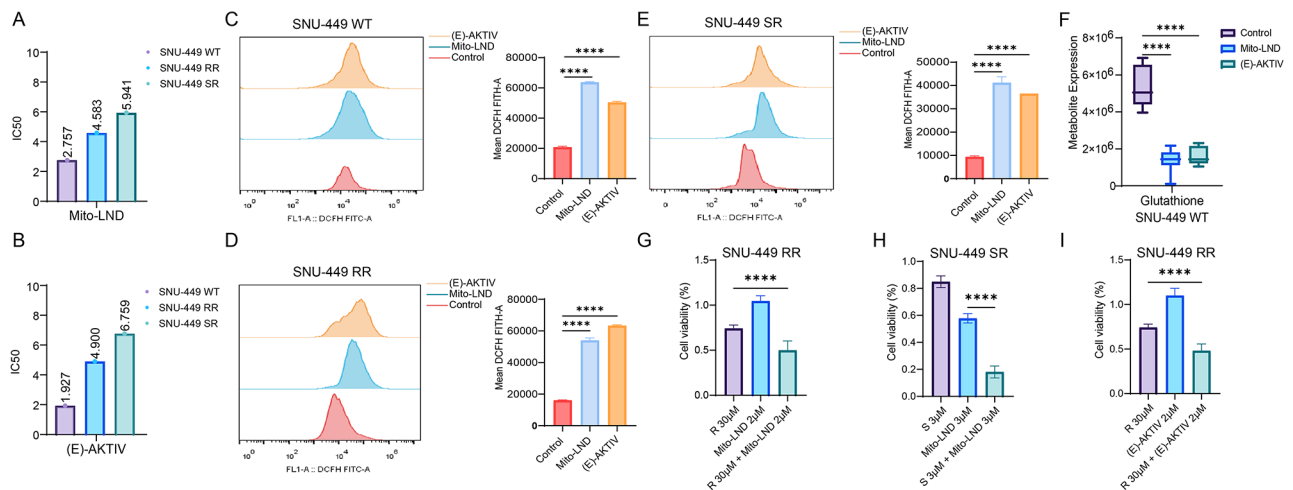

Fig. 2 Mito-LND and (E)-AKTIV increased ROS and decreased GSH in HCC cells. **A&B** In SNU-449 WT, SNU-449 RR, and SNU-449 SR cells, different concentrations of Mito-LND and (E)-AKTIV were added, and after 48 h of incubation, the IC50 values were obtained using the CCK-8 method. **C-E** In SNU-449 WT, SNU-449 RR, and SNU-449 SR cells, 4 μM of Mito-LND and (E)-AKTIV were added. After 48 h of incubation, 5 μM of DCFH-DA probe was introduced and incubated for an additional 30 min. Subsequently, the levels of ROS were measured using flow cytometry. **F** The metabolomic analysis revealed variations in GSH levels among Mito-LND, (E)-AKTIV, and the control group. **G-I** Using CCK-8 assay evaluated the cell viability after combined drug treatment. All the data were presented as means ± SD. **$P < 0.01$, ***$P < 0.001$, ****$P < 0.0001$

Liao *et al. Journal of Translational Medicine*   (2024) 22:792

Page 7 of 16

The results indicated a significant downregulation of GSH in SNU-449 WT upon the addition of Mito-LND and (E)-AKTIV (Fig. 2F). Simultaneously, in SNU-449 RR cells, the combination of regorafenib and Mito-LND displayed synergistic effects with a q value of 2.23, while in SNU-449 SR cells, the same drug combination showed synergy with a q value of 1.61. Moreover, the experimental results from combining sorafenib with (E)-AKTIV in the SNU-449 RR cell line also demonstrated synergism,

with a q value of 2.82 (Fig. 2G-I). The enrichment analysis showed that both drugs dramatically affected the glycolytic and TCA cycle pathways (Fig. 3A&B). As expected, metabolomics revealed a significant downregulation of citric acid, isocitric acid, and oxoglutaric acid (α-KG) in the Mito-LND group compared with unmedicated controls. D-Glycerate 3-Phosphate (G-3-P) and Beta-D-Glucose 6-phosphate (G-6-P) were instead upregulated in glycolysis (Fig. 3C). This suggested that Mito-LND
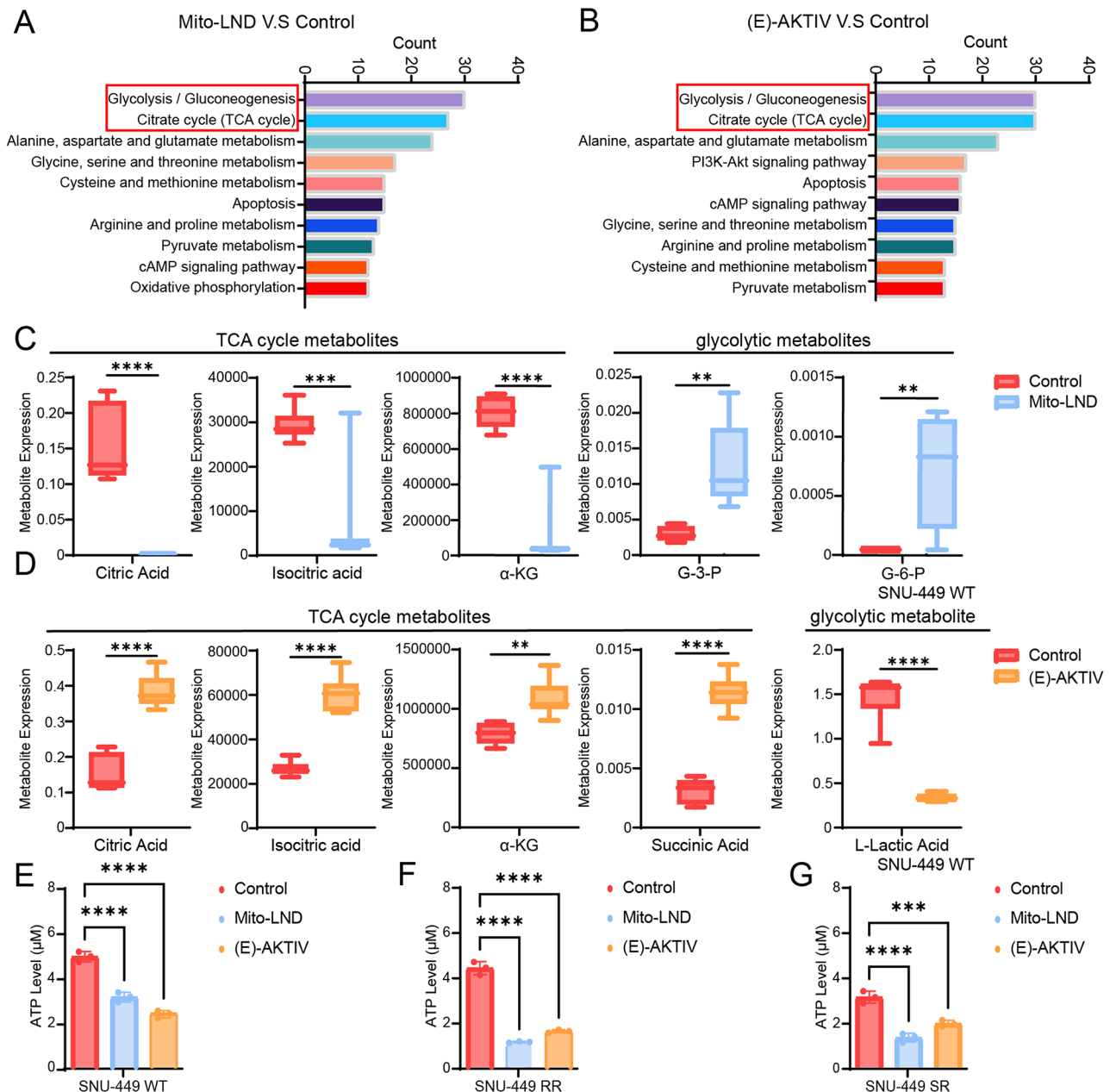

Fig. 3 Mito-LND inhibited tricarboxylic acid cycle, and (E)-AKTIV suppressed electron transport chain in HCC cells. **A&B** The metabolomic analysis revealed associations of Mito-LND and (E)-AKTIV with glycolysis and TCA cycle. **C&D** Metabolomic analysis revealed alterations in metabolites related to glycolysis and TCA cycle upon treatment with Mito-LND and (E)-AKTIV. E-G After treatment with 4 μM of Mito-LND and (E)-AKTIV for 48 h, ATP levels were measured. All the data were presented as means ± SD. ****$P < 0.0001$

seems to enhance glycolysis and attenuate the TCA cycle. On the other hand, we found TCA cycle metabolites, such as citric acid, isocitric acid, α-KG, and succinic acid increased, but glycolytic metabolites of L-lactic acid decreased in the (E)-AKTIV group (Fig. 3D), implying that (E)-AKTIV has opposite function to Mito-LND. Although the mechanism seems to be different, both drugs could result in a significant decrease in ATP levels across the three cell types (Fig. 3E-G). In sum, Mito-LND and (E)-AKTIV exert cytotoxic function on HCC Cells by increasing ROS level and imparing ATP synthesis.

Mito-LND and (E)-AKTIV effectively Induced apoptosis in HCC

ROS were the byproduct electron transport chains of mitochondria. High levels of ROS and the depletion of GSH indicated mitochondrial dysfunction, which was an important hallmark of apoptosis [19]. When SNU-449 WT, SNU-449 SR and SNU-449 RR cells were treated with 4 μM Mito-LND for 48 h in annexin V-FITC staining, the proportion of apoptotic cells was significantly higher as compared to the control (Fig. 4A-C). Like Mito-LND, (E)-AKTIV also induced increased apoptosis in both parental and drug-resistant cells (Fig. 4A-C). The reduced apoptosis rate in HCC-resistant cells compared to HCC wild-type cells is likely because drug-resistant cells have been associated with an apoptotic resistant phenotype [22].

Mito-LND and (E)-AKTIV effectively suppressed AMPK/AKT/MAPK signaling pathway

To reveal the molecular mechanism of these two drugs, we performed transcriptomic analysis after drug treatment. The subsequent kyoto encyclopedia of genes and
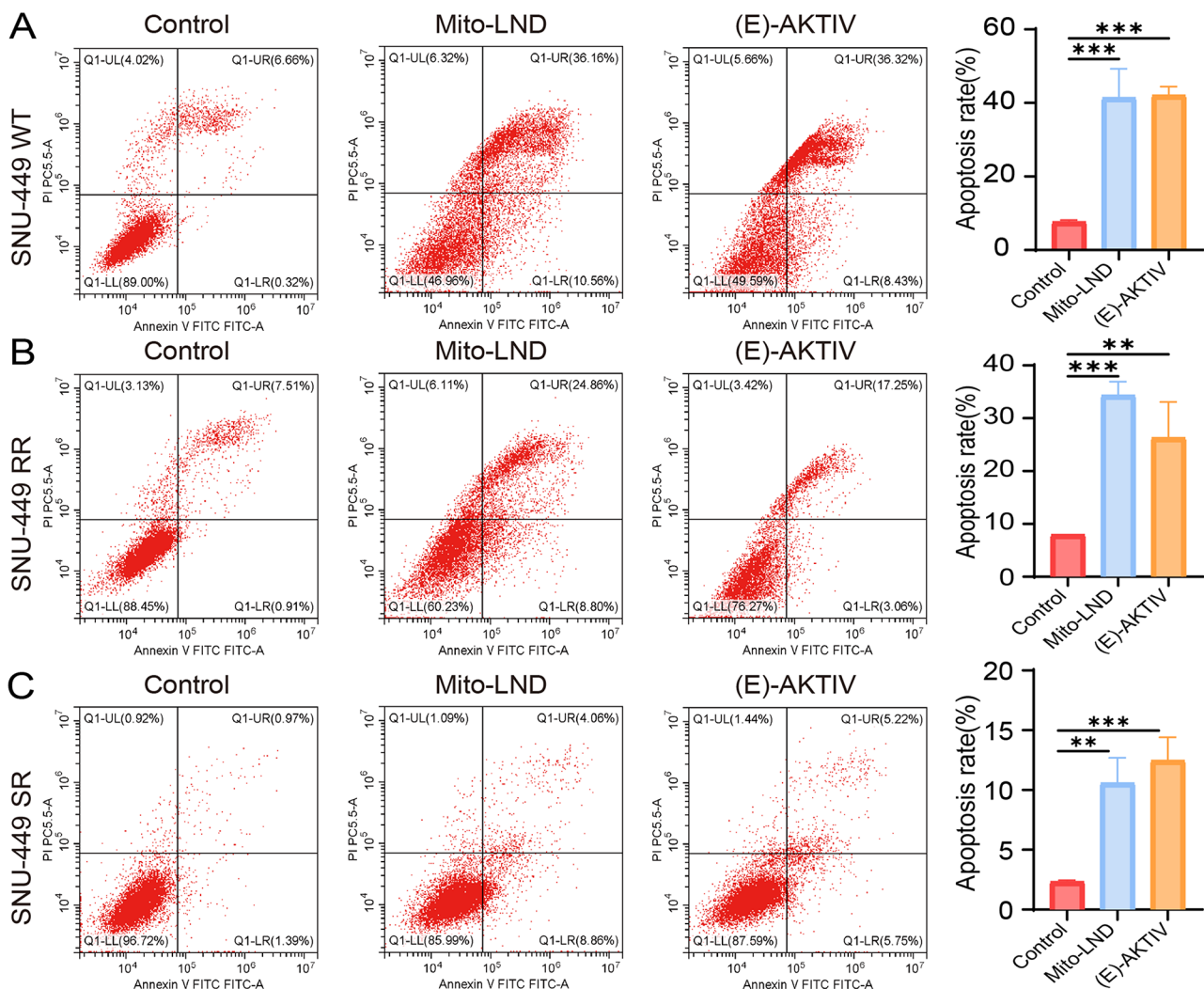

Fig. 4 Mito-LND and (E)-AKTIV induced apoptosis in both parental and resistant HCC cells. **A-C** After treating SNU-449 WT, SNU-449 RR, and SNU-449 SR cells with 4 μM of Mito-LND and (E)-AKTIV for 48 h, apoptosis rates were detected using flow cytometry. All the data were presented as means ± SD. **P < 0.01, ***P < 0.001
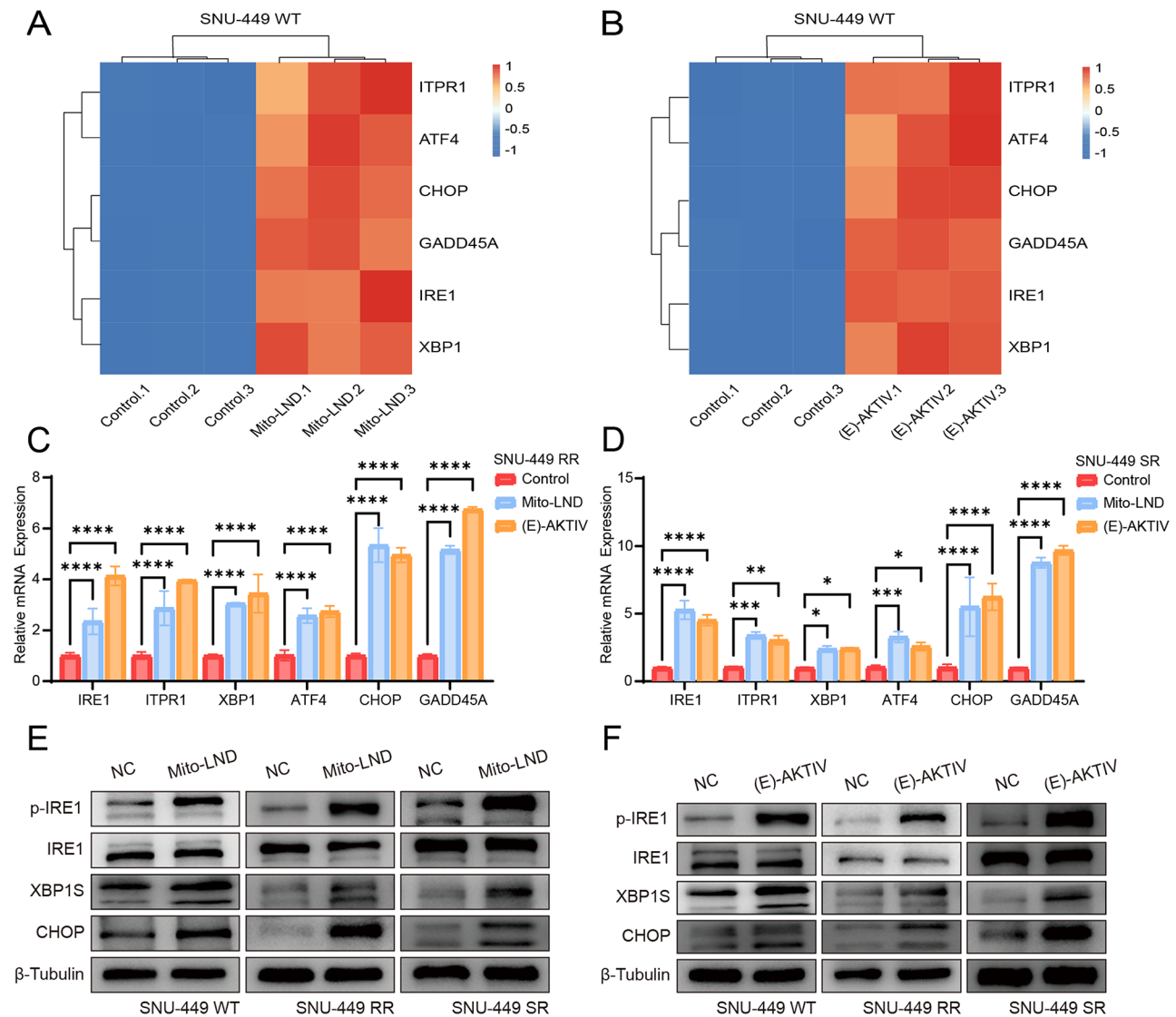
Fig. 6 Mito-LND and (E)-AKTIV induced endoplasmic reticulum stress in HCC cells. **A&B** Through transcriptome analysis, we identified upregulated genes associated with apoptosis in SNU-449 WT cells treated with Mito-LND and (E)-AKTIV. **C&D** Following treatment with 4μM of Mito-LND and (E)-AKTIV for 48 h, mRNA levels in both SNU-449 RR and SNU-449 SR cell lines were assessed. **E&F** After a 48-hour exposure to 4μM Mito-LND and (E)-AKTIV, protein levels of p-IRE, IRE, XBP1S, and CHOP were assessed using western blot analysis. All the data were presented as means ± SD. *$P < 0.05$, **$P < 0.01$, ***$P < 0.001$, ****$P < 0.0001$

genomes (KEGG) pathway analysis demonstrated that the apoptosis and MAPK signaling were significantly changed (Fig. 5A&B). Furthermore, gene set enrichment (GSEA) analysis also corroborated the same results (Fig. 5C&D). We have demonstrated that both compounds could affect the glycolysis, TCA cycle and ATP synthesis. Inhibition of mitochondrial respiration can induce energy stress and promote the activation of AMPK, which then leads to catabolism and restoration of energy homeostasis [23]. AMPK phosphorylation was increased in the drug groups as compared to the control group in SNU-449 SR, SNU-449 RR cells due to increased ROS and decreased ATP (Fig. 5E&F). Low level of mTOR

causes slower cell growth and reduced protein synthesis. Meanwhile, Phosphorylation of AKT regulates mTORC1 activation and inhibits apoptosis [24]. Same as in the previous study [17], Mito-LND and (E)-AKTIV reduced the level of phosphorylated AKT and mTOR in the three cells (Fig. 5E&F). There are a minimum of four MAPK subfamilies: extracellular signal-regulated kinase 1 and 2 (ERK1/2), Jun N-terminal kinases (JNKs), P38 MAPKs, and ERK5. MAPKs play a pivotal role in coordinating extracellular stimuli to regulate diverse cellular activities, including gene expression, cell proliferation, survival, and migration [25]. Phosphorylated MAPKs (ERK1/2, JNK, P38) levels were found significantly increased in
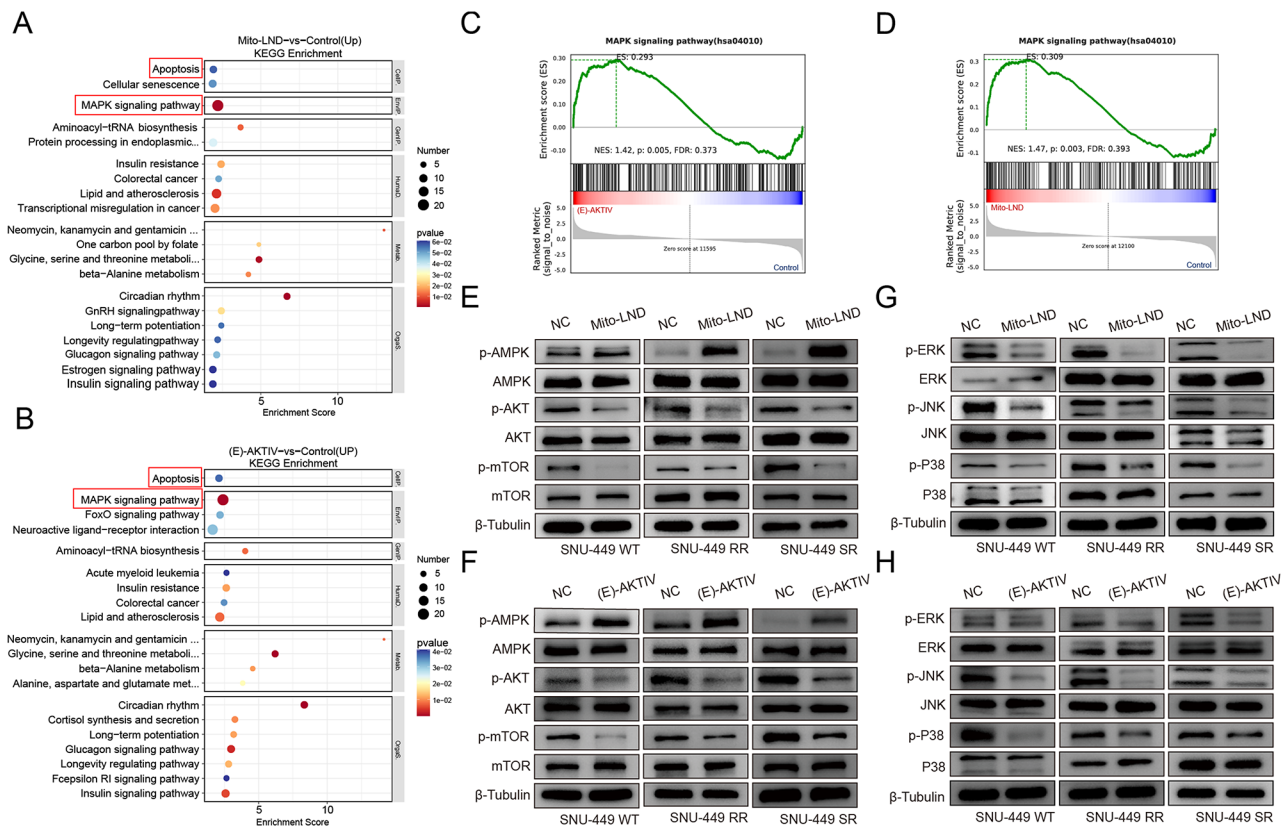
Fig. 5 Mito-LND and E-AKTIV depressed MAPK signaling while activate AMPK signaling. **A&B** Analysis of transcriptomic results using the KEGG database revealed associations of Mito-LND and (E)-AKTIV with apoptosis and the MAPK pathway. **C&D** Utilizing GSEA on transcriptomic data, significant associations were observed between the two drugs and the MAPK pathway. **E, F** After treatment with 4 μM of Mito-LND and (E)-AKTIV for 48 h, changes in the levels of p-AMPK, AMPK, p-AKT, AKT, p-mTOR and mTOR were assessed using western blot, in comparison to the control group. **G&H** After treating with 4 μM of Mito-LND and (E)-AKTIV for 48 h, changes in the levels of p-ERK, ERK, p-JNK, JNK, p-P38 and P38 were assessed using western blot, in comparison to the control group

most human HCC samples [26–28]. Activity of ERK has been shown to inhibit apoptosis, promote proliferation and increase survival [29, 30]. Interestingly, our study found that the phosphorylation levels of MAPK (including ERK1/2, JNK and P38) were reduced, inhibiting cell growth and proliferation, and promoting apoptosis in Mito-LND and (E)-AKTIV treated SNU-449 WT cells (Fig. 5G&H). To reaffirm the association between the MAPK signaling pathway and the inhibition of HCC cell growth by Mito-LND and (E)-AKTIV, we treated drug-resistant HCC cells with these compounds. By subjecting resistant cells to the influence of both drugs, we reevaluated the inhibitory impact of Mito-LND and (E)-AKTIV on the signaling pathway in HCC cells. Western blot analysis showed that phosphorylated ERK1/2, JNK, and P38 were all significantly reduced (Fig. 5G&H). Overall, Mito-LND and (E)-AKTIV reduced cell proliferation and promoted apoptosis of parental cells and drug-resistant cells through AMPK/AKT/MAPK pathways in HCC. Mutual crosstalk of these pathways enhances the apoptotic death of HCC cells in vitro.

Mito-LND and (E)-AKTIV triggered ER stress and activated the IRE1-XBP1-CHOP Axis to induce intrinsic apoptosis

Increased protein secretion or disruption of endoplasmic reticulum (ER) protein folding causes the accumulation of unfolded or misfolded proteins in the ER lumen — a condition known as "ER stress". Protein misfolding following overexpression of secretory proteins triggers the unfolded protein response (UPR), which promotes stress adaptation [31]. Increased ROS generation, hypoxia, nutrient deprivation, chemotherapeutic drug exposure, and improper calcium homeostasis can cause the UPR [32]. Induction of ER stress and activation of the UPR impairs the epithelial cell phenotype transition and the development of apoptosis [33]. The transcriptome results in SNU-449 WT showed that inositol requiring enzyme 1 (IRE1), activating transcription factor 4 (ATF4), transcription factor C/EBP orthologue (CHOP) and x-box binding protein 1 (XBP1) were significantly increased in the UPR pathway. In addition, pro-apoptosis genes such as inositol 1,4,5-trisphosphate receptor, type 1 (ITPR1), growth arrest and DNA damage-inducible α (GADD45A) were upregulated (Fig. 6A&B). Consistent with the

transcriptomic results, the Real-time quantitative PCR (RT-qPCR) results showed that the mRNA expression of IRE1, XBP1, ATF4, CHOP, ITPR1, GADD45A all increased in SNU-449 SR and SNU-449 RR after treatment (Fig. 6C&D). We further validated that p-IRE1, spliced XBP1(XBP1S), and CHOP protein levels in the UPR pathway were significantly increased in both drugs as compared with the control group (Fig. 6E&F). This showed that parental cells promote apoptosis through the same signaling pathway as resistant cells.

Anticancer effect of Mito-LND and (E)-AKTIV in vivo

In view of the good cytotoxic function of the above two drugs in vitro, we performed the validation in athymic nude mice. Briefly, SK-Hep1 cells (5×10^6) were injected subcutaneously into the right flank of athymic nude mice. One week after injection, mice were treated with the same dose of Mito-LND or (E)-AKTIV (100 μmol/kg) or vehicle (administered saline+DMSO) by subcutaneous injection for 3 weeks (Fig. 7A). We choose subcutaneous injection due to the strong side effect of these drugs in peritoneal injection model. The tumor volume and weight were significantly reduced relative to the control group upon sustained stimulation with Mito-LND and (E)-AKTIV (Fig. 7B-D). In continuous observations, Mito-LND reduced the growth rate of SK-Hep1 tumor xenografts, maintained the tumor volume and kept them silent (Fig. 7E). However, (E)-AKTIV significantly reduced the tumor size and seems to show a stronger tumor killer in *vivo*. Histological examination with hematoxylin and eosin (H&E) staining revealed an increased incidence of cell necrosis in both drug-treated groups. Concurrently, histological and immunohistochemical (IHC) experiments demonstrated elevated expression levels of p-IRE1, CHOP, and XBP1 in tissues treated with Mito-LND and (E)-AKTIV, suggesting an induction of cell apoptosis through ER stress (Fig. 7F). Concurrently, we conducted an orthotopic tumor formation experiment in NCG mice, administering gavage treatment for three weeks (Fig. 7A). Initiated with 9 NCG mice per group, post-treatment outcomes revealed a mortality of 6 in the control, 3 in Mito-LND, and 4 in (E)-AKTIV groups, underscoring superior survival rates in the treated cohorts relative to controls (Fig. 7G). Through in vivo imaging, we observed that the mean bioluminescence intensity of hepatic tumors and pulmonary metastases was lower in the treatment groups compared to controls, indicating suppressed tumor growth (Fig. 7H-J). Despite a general decline in body weight over time across all mice, no significant inter-group differences in weight were noted (Fig. 7K). Further H&E staining confirmed the absence of drug-induced damage to major organs, affirming the safety of the treatments (Fig. 7L). Our findings demonstrate that Mito-LND and (E)-AKTIV effectively suppress HCC cell growth in *vivo*, and that they can have the potential to be safe and effective anticancer agents.

Discussion

HCC is one of the most lethal cancers worldwide [34]. The intrinsic or acquired drug resistance is the main reason for treatment failure. More and more evidence showed that targeting cancer metabolism could be an effective way to enhance the therapeutic efficacy. We herein successfully established sorafenib-resistant and regorafenib-resistant HCC cells and screened two mitochondria targeted drugs (Mito-LND and (E)-AKTIV) in SK-Hep 1, Huh7, SNU-449, and SNU-449 RR cells by anti-cancer metabolism compound library. Previous research has indicated that Mito-LND can impede cells in the G0/G1 phase, leading to the inhibition of cell proliferation [18]. Additionally, Mito-LND has been observed to suppress the activity of mitochondrial respiratory chain complex I, leading to a reduction in mitochondrial membrane potential and subsequently promoting ROS production [17, 18]. It can also induce apoptosis and autophagy in cancer cells [17, 18]. Mechanistically, cancer cell proliferation was reduced by inactivating AKT/mTOR/p70S6K signaling and blocking Raf/MEK/ERK signaling in lung cancer and glioma, respectively [17, 18]. (E)-AKTIV is similar to Mito-LND in some parts, both as mitochondrial depolarization, reduced mitochondrial respiration and release of ROS [19]. We found that both Mito-LND and (E)-AKTIV could impair glycolysis and TCA cycle in HCC cells, thus suppressing ATP synthesis and inducing ROS accumulation.

Glycolysis and TCA cycle coupled to the electron transport chain can provide ATP to supply cellular energy [35]. Cancer cells generally exhibit an enhanced ability to take up glucose from the extracellular environment to meet its energetic requirements. However, most cancer cells breathe through the TCA cycle to promote tumor growth. In the past decade, the TCA cycle has also returned as a key anabolic center supporting tumor growth. Mitochondria, as sites where TCA cycling occurs, not only support ATP generation but also participate in redox and calcium homeostasis, transcriptional regulation and control of cell death [36]. Therefore, targeting mitochondrial metabolism holds promise for the development of innovative anti-tumor agents. The main sources of ROS are lipid peroxidation of the mitochondrial respiratory chain, and mitochondrial polyunsaturated membranes. Although excessive proliferation of tumor cells is accompanied by high ROS production, high ROS levels are cytotoxic [37]. Excess ROS, triggered by pathological or pharmacological factors, can lead to mitochondrial dysfunction, reduced ATP, lipid peroxidation, and DNA damage, ultimately inhibiting cell growth or promoting cell death [38]. Our previous study also
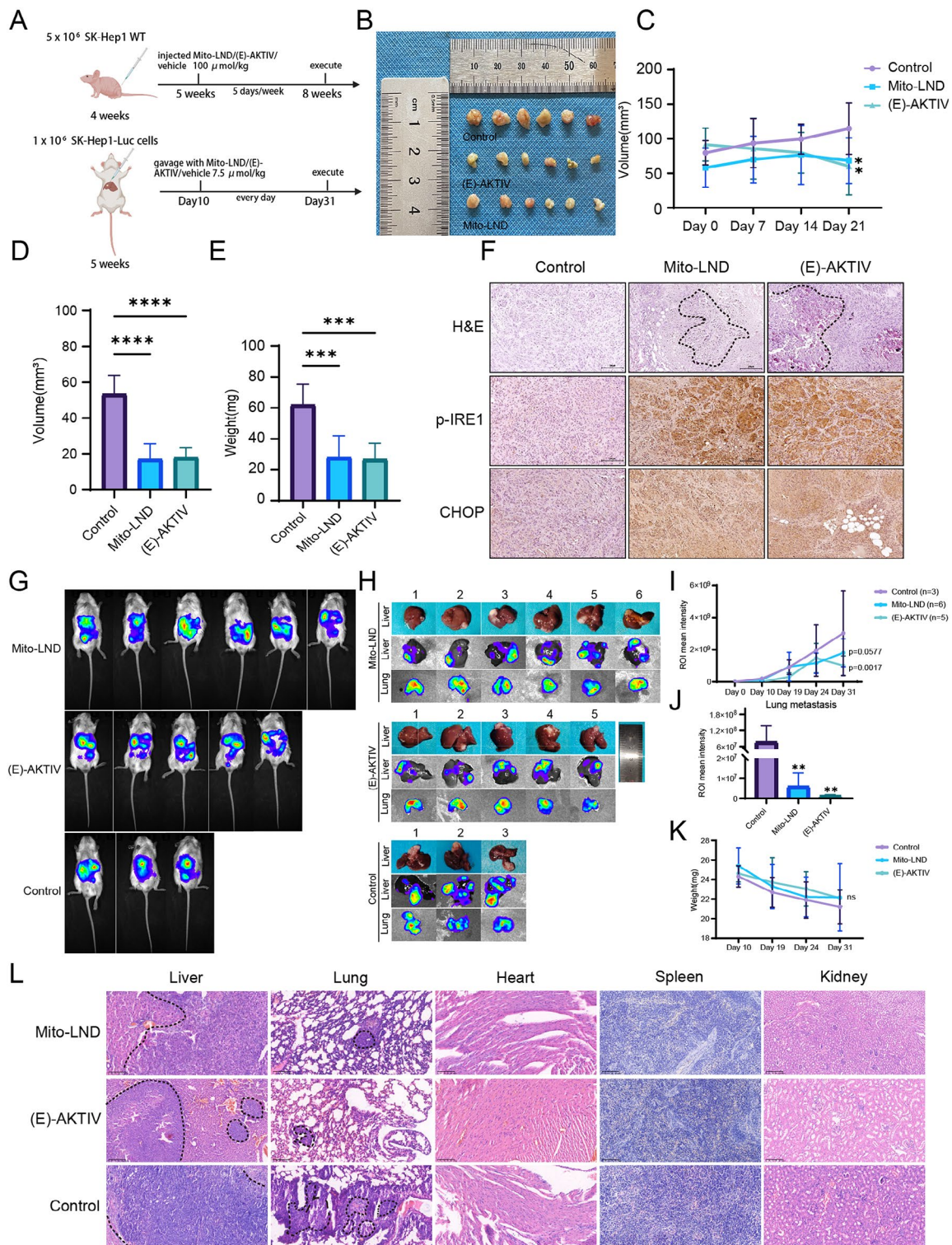
Fig. 7 Mito-LND and (E)-AKTIV suppressed the growth of HCC cells in vivo via inducing ER stress. **A** The flowchart of nude/NCG mice drug administration. **B-E** Record tumor volume and body weight post-administration, with continuous monitoring of tumor volume. **F** Perform H&E and IHC staining for Mito-LND, (E)-AKTIV, and the control group, scale bar: 200 μm. **G&H** Live imaging of NCG mice and post-mortem imaging of livers and lungs from the mice. **I** The mean bioluminescence intensity in NCG mice across the Mito-LND, (E)-AKTIV, and control groups. J The weight of NCG mice. **K** The mean bioluminescence intensity in the lungs of NCG mice. **L** H&E stained images of the liver, lungs, heart, spleen, and kidneys from NCG mice, scale bar: 200 μm. The dashed areas denote the regions of hepatic in situ tumors and pulmonary metastatic lesions. All the data were presented as means ± SD. *$P < 0.05$, ***$P < 0.001$, ****$P < 0.0001$

showed that nuclear factor NFIB could transcriptionally upregulate Complex I subunit NDUFV4 to reduce sorafenib-induced ROS level [39].

Lonidamine (LND), owing to its low toxicity and targeted approach to energy metabolism, holds promise for augmenting the efficacy of therapeutic agents in clinical cancer treatment [40]. Mito-LND is synthesized by conjugating a long alkyl chain to triphenylphosphonium cation and linking it to LND [41]. Mito-LND can cause mitochondrial swelling, decrease mitochondrial membrane potential, weakened complex I activity and decreased GSH activity, and many factors can increase ROS [17, 18]. (E)-AKTIV acts in a manner similar to AKTIV, causing mitochondrial swelling and mitochondrial depolarization and promoting the production of ROS [18]. Notably, our results also confirmed that Mito-LND and (E)-AKTIV can promote ROS production in HCC parental and drug-resistant cells. ROS serves as a potent trigger for apoptosis, activating the intrinsic mitochondrial pathway, extrinsic death receptor pathway, and ER stress pathway [42]. And prolonged ER stress has overoxidized the ER lumen, which may lead to the leakage of H_2O_2 into the cytoplasm and directly induce ROS in the cytoplasm [43]. When the capacity of the UPR to maintain proteostasis is exceeded, cells initiate apoptotic programs [44]. IRE1α, double-stranded RNA activated protein kinase-like ER kinase (PERK), and activated transcription factor 6 (ATF6) were identified as UPR transducers [31]. Our study showed that ROS prompted the ER pathway activation of IRE1-XBP1-CHOP to induce apoptosis in HCC (Fig. 8). IRE1α, a Ser/Thr kinase and endoribonuclease, activates unconventional splicing of XBP1 mRNA upon induction. This leads to increased expression of XBP1s, which in turn regulates a broad array of UPR genes involved in protein folding, ER entry, redox balance, ERAD, and protein quality control [45]. CHOP is not only a transcriptional target of ATF4, but also that of XBP1 and ATF6 [44]. IRE1α also binds to adaptor proteins and has crosstalk with other stress response pathways (including macroautophagy and MAPK pathways) [46]. JNK activation caused increased expression of anti-apoptotic proteins (cIap 1, cIap 2, and XIap) and decreased ER-induced cell death [47].

Mechanistically, the accumulation of ROS and decrease in ATP activate multiple pathways and can have differential effects on cancer cell survival. AMPK acts as an energy-sensing factor that rewiring metabolism and maintain redox balance [48]. As a proto-oncogene, AKT contributes to cancer development and progression by primarily enhancing cell survival and suppressing apoptosis. Notably, AKT counteracts the role of AMPK in ROS-induced apoptosis. AMPK suppresses mTORC1 activity, thereby decreasing protein synthesis and augmenting autophagy. Inversely, AKT activates mTOR by inhibiting TSC2, enabling Rheb-GAP to phosphorylate mTORC1 [49]. In addition, AMPK reversely inhibits AKT phosphorylation [50]. Our study showed that Mito-LND and (E)-AKTIV increased AMPK phosphorylation and inhibited the phosphorylation of AKT and mTOR. This explains part of the increase of ROS in HCC wild-type cells as well as in drug-resistant cells.

Over the past few decades, massive studies have shown that MAPK plays a key role in transforming extracellular stimuli into a wide range of cellular responses (including cell growth, migration, proliferation, differentiation, and apoptosis). ERK 1/2 plays a central role in the control of
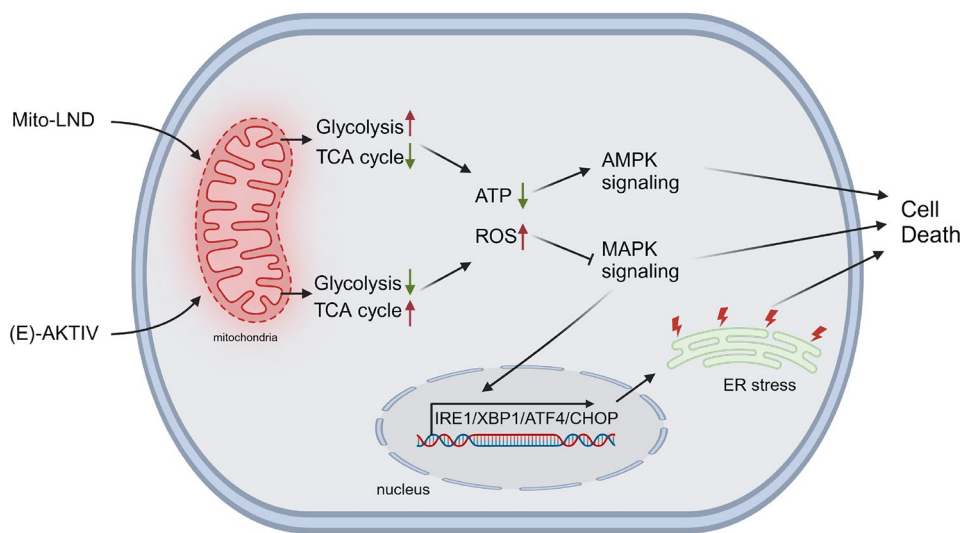

Fig. 8 Mechanism diagrams of Mito-LND and (E)-AKTIV. Mito-LND increases mitochondrial glycolysis, decreases TCA cycle products, leading to reduced ATP and increased ROS. In contrast, (E)-AKTIV reduces mitochondrial glycolysis, increases TCA cycle products, resulting in decreased ATP and elevated ROS. Both drugs activate the AMPK/MAPK pathway and involve ER proteins in endoplasmic reticulum stress

cell proliferation [51]. Meanwhile, JNK and P38 activation regulate apoptosis [52]. On the one hand, numerous studies have reported the positive effects of JNK and P38 in pro-apoptosis [53–55]. On the other hand, JNK and P38 have shown anti-apoptotic potential in some studies [56, 57]. In our study, ERK 1/2, JNK and P38 phosphorylation level were all down-regulated in Mito-LND and (E)-AKTIV treated HCC cells. However, the specific mechanism of JNK and P38 on pro-apoptosis in HCC remains unclear. We further demonstrated that Mito-LND and (E)-AKTIV reduce ATP production and increase ROS accumulation through the interaction of AMPK/AKT/MAPK and ER stress pathways, thereby promoting apoptosis of HCC parental and drug-resistant cells (Fig. 8). However, the specific regulatory mechanisms affecting glycolysis, TCA cycle and GSH need to be further explored in the following studies. However, we speculate that due to the targeting characteristics of these two drugs, this may be closely related to mitochondrial dysfunction. Therefore, the mechanisms by which Mito-LND and (E)-AKTIV inhibit tumor growth and promote apoptosis deserve further investigation. Furthermore, the combined use of sorafenib/regorafenib with Mito-LND or (E)-AKTIV demonstrates a synergistic inhibitory effect against HCC. 3-Bromopyruvate optimizes the efficacy of chloroethyl nitrosourea in the treatment of hepatocellular carcinoma, due to its potent inhibitory effect on glycolysis [58]. 2-Deoxy-D-glucose may potentiate the metabolic vulnerability of glioblastoma cells to 1,3-bis(2-chloroethyl)-1-nitrosourea by modulating glycolysis, ROS, and ER stress pathways [59]. These suggest that the combination of energy metabolism inhibitors with anti-tumor drugs may also augment the therapeutic efficacy against HCC.

In *vivo* experiments reveal that Mito-LND and (E)-AKTIV markedly inhibit hepatic tumor growth and reduce lung metastasis incidence. Notably, mice that did not survive to the study endpoint exhibited larger tumor volumes. Bioluminescence imaging of the mice's livers showed a decrease in fluorescence values, albeit without reaching statistical significance (Figure S2). This may be attributed to the drugs' enhanced efficacy in suppressing pulmonary metastases. H&E staining combined with body weight monitoring indicates that these drugs exhibit no significant adverse effects on major organ function and body weight, highlighting their safety and outstanding antitumor efficacy.

Conclusions

Mitochondria-focused drugs, Mito-LND and (E)-AKTIV, have shown promise in slowing the growth of both wild-type and drug-resistant tumor cells in HCC. These compounds also decrease ATP production, increase ROS level, and trigger apoptosis by targeting *AMPK/AKT/MAPK* and *IRE1-XBP1-CHOP* pathway. Furthermore, they exhibit strong anti-tumor effects and biological safety in *vivo* experiments. These characteristics suggest that these compounds could potentially become the cornerstone of a new treatment regimen or play a crucial role in developing drugs that extend patient lifespans by overcoming drug resistance in HCC.

Abbreviations

HCC	Hepatocellular carcinoma
ATP	Adenosine triphosphate
ROS	Reactive oxygen species
TCA	Tricarboxylic acid
SDH	Succinate dehydrogenase
Mito-LND	Mito-lonidamine
(E)-AKTIV	(E)-Akt inhibitor-IV
SNU-449 WT	SNU-449 wild-type cells
CCK-8	Cell counting kit-8 assay
SNU-449 RR	SNU-449 regorafenib-resistant cells
SNU-449 SR	SNU-449 sorafenib-resistant cells
H&E	Hematoxylin and Eosin
IHC	Immunohistochemistry
IC50	The lowest half maximal inhibitory concentration
SK-Hep1 WT	SK-Hep1 wild-type cells
Huh7 WT	Huh7 wild-type cells
GSH	Glutathione
α-KG	Oxoglutaric acid
G-3-P	D-Glycerate 3-Phosphate
G-6-P	Beta-D-Glucose 6-phosphate
KEGG	Kyoto encyclopedia of genes and genomes
GSEA	Gene set enrichment
ER	Endoplasmic reticulum
UPR	Unfolded protein response
IRE1	Inositol requiring enzyme 1
ATF4	Activating transcription factor 4
CHOP	Transcription factor C/EBP orthologue
XBP1	X-box binding protein 1
ITPR1	Inositol 1,4,5-trisphosphate receptor, type 1
GADD45A	DNA damage-inducibleα
RT-qPCR	Real-time quantitative PCR
XBP1S	Spliced XBP1
LND	Lonidamine
PERK	Protein kinase-like ER kinase
ATF6	Transcription factor 6

Supplementary Information

The online version contains supplementary material available at https://doi.org/10.1186/s12967-024-05545-5.

Supplementary Material 1

Supplementary Material 2

Declarations

Ethics approval and consent to participate
All animal experimental protocols were approved by the Animal Ethic Committee of the Second Affiliated Hospital of Chongqing Medical University.

Consent for publication
Not applicable.

Competing interests
Authors have no relevant financial or non-financial interests to disclose.

Author details
[1]The Department of Gastroenterology, The Second Affiliated Hospital of Chongqing Medical University, Chongqing, China
[2]The Department of Pathology, The Second Affiliated Hospital of Chongqing Medical University, Chongqing, China
[3]The Department of Endocrinology, The Second Affiliated Hospital of Chongqing Medical University, Chongqing, China

References

1. Ladd AD, Duarte S, Sahin I et al. Mechanisms of drug resistance in HCC. *Hepatology* 2023. https://doi.org/10.1097/HEP.0000000000000237
2. Germano D, Daniele B. Systemic therapy of hepatocellular carcinoma: current status and future perspectives. World J Gastroenterol. 2014;20(12):3087–99. https://doi.org/10.3748/wjg.v20.i12.3087.
3. Chan SL, Wong N, Lam WKJ, et al. Personalized treatment for hepatocellular carcinoma: current status and future perspectives. J Gastroenterol Hepatol. 2022;37(7):1197–206. https://doi.org/10.1111/jgh.15889.
4. Hanahan D. Hallmarks of Cancer: New dimensions. Cancer Discov. 2022;12(1):31–46. https://doi.org/10.1158/2159-8290.CD-21-1059.
5. Warburg O. On respiratory impairment in cancer cells. Science. 1956;124(3215):269–70.
6. Martínez-Reyes I, Chandel NS. Cancer metabolism: looking forward. Nat Rev Cancer. 2021;21(10):669–80. https://doi.org/10.1038/s41568-021-00378-6.
7. Xiao Y, Yu T-J, Xu Y, et al. Emerging therapies in cancer metabolism. Cell Metab. 2023;35(8):1283–303. https://doi.org/10.1016/j.cmet.2023.07.006.
8. Farber S, Diamond LK. Temporary remissions in acute leukemia in children produced by folic acid antagonist, 4-aminopteroyl-glutamic acid. N Engl J Med. 1948;238(23):787–93.
9. Stine ZE, Schug ZT, Salvino JM, et al. Targeting cancer metabolism in the era of precision oncology. Nat Rev Drug Discov. 2022;21(2):141–62. https://doi.org/10.1038/s41573-021-00339-6.
10. Zong W-X, Rabinowitz JD, White E. Mitochondria and Cancer. Mol Cell. 2016;61(5):667–76. https://doi.org/10.1016/j.molcel.2016.02.011.
11. Yun J, Mullarky E, Lu C, et al. Vitamin C selectively kills KRAS and BRAF mutant colorectal cancer cells by targeting GAPDH. Science. 2015;350(6266):1391–96. https://doi.org/10.1126/science.aaa5004.
12. Pollak M. Potential applications for biguanides in oncology. J Clin Invest. 2013;123(9):3693–700. https://doi.org/10.1172/JCI67232.
13. Cardaci S, Zheng L, MacKay G, et al. Pyruvate carboxylation enables growth of SDH-deficient cells by supporting aspartate biosynthesis. Nat Cell Biol. 2015;17(10):1317–26. https://doi.org/10.1038/ncb3233.
14. Buchdunger E, Zimmermann J, Mett H, et al. Inhibition of the abl protein-tyrosine kinase in vitro and in vivo by a 2-phenylaminopyrimidine derivative. Cancer Res. 1996;56(1):100–04.
15. Hynes NE, Lane HA. ERBB receptors and cancer: the complexity of targeted inhibitors. Nat Rev Cancer. 2005;5(5):341–54.
16. Jin Z-j. About the evaluation of drug combination. Acta Pharmacol Sin. 2004;25(2):146–47.
17. Cheng G, Zhang Q, Pan J, et al. Targeting lonidamine to mitochondria mitigates lung tumorigenesis and brain metastasis. Nat Commun. 2019;10(1):2205. https://doi.org/10.1038/s41467-019-10042-1.
18. Guo T, Wu C, Zhou L, et al. Preclinical evaluation of Mito-LND, a targeting mitochondrial metabolism inhibitor, for glioblastoma treatment. J Transl Med. 2023;21(1):532. https://doi.org/10.1186/s12967-023-04332-y.
19. Meinig JM, Peterson BR. Anticancer/antiviral agent akt inhibitor-IV massively accumulates in mitochondria and potently disrupts cellular bioenergetics. ACS Chem Biol. 2015;10(2):570–76. https://doi.org/10.1021/cb500856c.
20. Zitka O, Skalickova S, Gumulec J, et al. Redox status expressed as GSH:GSSG ratio as a marker for oxidative stress in paediatric tumour patients. Oncol Lett. 2012;4(6):1247–53.
21. Franco R, DeHaven WI, Sifre MI, et al. Glutathione depletion and disruption of intracellular ionic homeostasis regulate lymphoid cell apoptosis. J Biol Chem. 2008;283(52):36071–87. https://doi.org/10.1074/jbc.M807061200.
22. Friesen C, Kiess Y, Debatin KM. A critical role of glutathione in determining apoptosis sensitivity and resistance in leukemia cells. Cell Death Differ. 2004;11(Suppl 1):S73–85.
23. Choi YK, Park K-G. Metabolic roles of AMPK and metformin in cancer cells. Mol Cells. 2013;36(4):279–87. https://doi.org/10.1007/s10059-013-0169-8.
24. Thoreen CC, Chantranupong L, Keys HR, et al. A unifying model for mTORC1-mediated regulation of mRNA translation. Nature. 2012;485(7396):109–13. https://doi.org/10.1038/nature11083.
25. Huang P, Han J, Hui L. MAPK signaling in inflammation-associated cancer development. Protein Cell. 2010;1(3):218–26. https://doi.org/10.1007/s13238-010-0019-9.
26. Lee HC, Tian B, Sedivy JM, et al. Loss of raf kinase inhibitor protein promotes cell proliferation and migration of human hepatoma cells. Gastroenterology. 2006;131(4):1208–17.
27. Guo L, Guo Y, Xiao S, et al. Protein kinase p-JNK is correlated with the activation of AP-1 and its associated Jun family proteins in hepatocellular carcinoma. Life Sci. 2005;77(15):1869–78.
28. Devarbhavi H, Asrani SK, Arab JP, et al. Global burden of liver disease: 2023 update. J Hepatol. 2023;79(2):516–37. https://doi.org/10.1016/j.jhep.2023.03.017. [published Online First: 20230327].
29. Dajee M, Tarutani M, Deng H, et al. Epidermal Ras blockade demonstrates spatially localized Ras promotion of proliferation and inhibition of differentiation. Oncogene. 2002;21(10):1527–38.
30. Tran SE, Holmstrom TH, Ahonen M, et al. MAPK/ERK overrides the apoptotic signaling from Fas, TNF, and TRAIL receptors. J Biol Chem. 2001;276(19):16484–90.
31. Hetz C, Zhang K, Kaufman RJ. Mechanisms, regulation and functions of the unfolded protein response. Nat Rev Mol Cell Biol. 2020;21(8):421–38. https://doi.org/10.1038/s41580-020-0250-z.
32. Riaz TA, Junjappa RP, Handigund M, et al. Role of endoplasmic reticulum stress sensor IRE1α in Cellular Physiology, Calcium, ROS Signaling, and metaflammation. Cells. 2020;9(5). https://doi.org/10.3390/cells9051160.
33. Cybulsky AV. Endoplasmic reticulum stress, the unfolded protein response and autophagy in kidney diseases. Nat Rev Nephrol. 2017;13(11):681–96. https://doi.org/10.1038/nrneph.2017.129.
34. Yang Z, Zhou L, Si T, et al. Lysyl hydroxylase LH1 promotes confined migration and metastasis of cancer cells by stabilizing Septin2 to enhance actin network. Mol Cancer. 2023;22(1):21. https://doi.org/10.1186/s12943-023-01727-9.
35. Kato Y, Maeda T, Suzuki A, et al. Cancer metabolism: new insights into classic characteristics. Jpn Dent Sci Rev. 2018;54(1). https://doi.org/10.1016/j.jdsr.2017.08.003.
36. Vasan K, Werner M, Chandel NS. Mitochondrial metabolism as a target for Cancer Therapy. Cell Metab. 2020;32(3):341–52. https://doi.org/10.1016/j.cmet.2020.06.019.
37. Reczek CR, Birsoy K, Kong H, et al. A CRISPR screen identifies a pathway required for paraquat-induced cell death. Nat Chem Biol. 2017;13(12):1274–79. https://doi.org/10.1038/nchembio.2499.
38. Gorrini C, Harris IS, Mak TW. Modulation of oxidative stress as an anticancer strategy. Nat Rev Drug Discov. 2013;12(12):931–47. https://doi.org/10.1038/nrd4002.
39. Zhou L, Mao L-H, Li X, et al. Transcriptional regulation of NDUFA4L2 by NFIB induces sorafenib resistance by decreasing reactive oxygen species

Liao *et al. Journal of Translational Medicine*   (2024) 22:792

Page 16 of 16

in hepatocellular carcinoma. Cancer Sci. 2023;114(3):793–805. https://doi.org/10.1111/cas.15648.

40. Huang Y, Sun G, Sun X, et al. The potential of Lonidamine in combination with chemotherapy and physical therapy in Cancer Treatment. Cancers (Basel). 2020;12(11). https://doi.org/10.3390/cancers12113332.

41. Zielonka J, Joseph J, Sikora A, et al. Mitochondria-targeted triphenylphosphonium-based compounds: syntheses, mechanisms of Action, and therapeutic and diagnostic applications. Chem Rev. 2017;117(15):10043–120. https://doi.org/10.1021/acs.chemrev.7b00042.

42. Redza-Dutordoir M, Averill-Bates DA. Activation of apoptosis signalling pathways by reactive oxygen species. Biochim Biophys Acta. 2016;1863(12):2977–92. https://doi.org/10.1016/j.bbamcr.2016.09.012.

43. Marciniak SJ, Yun CY, Oyadomari S, et al. CHOP induces death by promoting protein synthesis and oxidation in the stressed endoplasmic reticulum. Genes Dev. 2004;18(24):3066–77.

44. Ron D, Walter P. Signal integration in the endoplasmic reticulum unfolded protein response. Nat Rev Mol Cell Biol. 2007;8(7):519–29.

45. Uemura A, Oku M, Mori K, et al. Unconventional splicing of XBP1 mRNA occurs in the cytoplasm during the mammalian unfolded protein response. J Cell Sci. 2009;122(Pt 16):2877–86. https://doi.org/10.1242/jcs.040584.

46. Hetz C, Papa FR. The unfolded protein response and cell Fate Control. Mol Cell. 2018;69(2):169–81. https://doi.org/10.1016/j.molcel.2017.06.017.

47. Brown M, Strudwick N, Suwara M, et al. An initial phase of JNK activation inhibits cell death early in the endoplasmic reticulum stress response. J Cell Sci. 2016;129(12):2317–28. https://doi.org/10.1242/jcs.179127.

48. Hardie DG, Ross FA, Hawley SA. AMPK: a nutrient and energy sensor that maintains energy homeostasis. Nat Rev Mol Cell Biol. 2012;13(4):251–62. https://doi.org/10.1038/nrm3311.

49. Manning BD, Cantley LC. AKT/PKB signaling: navigating downstream. Cell. 2007;129(7):1261–74.

50. King TD, Song L, Jope RS. AMP-activated protein kinase (AMPK) activating agents cause dephosphorylation of akt and glycogen synthase kinase-3. Biochem Pharmacol. 2006;71(11):1637–47.

51. Meloche S, Pouysségur J. The ERK1/2 mitogen-activated protein kinase pathway as a master regulator of the G1- to S-phase transition. Oncogene. 2007;26(22):3227–39.

52. Yue J, López JM. Understanding MAPK signaling pathways in apoptosis. Int J Mol Sci. 2020;21(7). https://doi.org/10.3390/ijms21072346.

53. Sendoel A, Maida S, Zheng X, et al. DEPDC1/LET-99 participates in an evolutionarily conserved pathway for anti-tubulin drug-induced apoptosis. Nat Cell Biol. 2014;16(8):812–20. https://doi.org/10.1038/ncb3010.

54. Ji K-Y, Kim KM, Kim YH, et al. Serum starvation sensitizes Anticancer Effect of Anemarrhena asphodeloides via p38/JNK-Induced cell cycle arrest and apoptosis in Colorectal Cancer cells. Am J Chin Med. 2021;49(4):1001–16. https://doi.org/10.1142/S0192415X21500488.

55. Xiong J-X, Li Y-T, Tan X-Y, et al. Targeting PRSS23 with tipranavir induces gastric cancer stem cell apoptosis and inhibits growth of gastric cancer via the MKK3/p38 MAPK-IL24 pathway. Acta Pharmacol Sin. 2023. https://doi.org/10.1038/s41401-023-01165-9.

56. Yu C, Minemoto Y, Zhang J, et al. JNK suppresses apoptosis via phosphorylation of the proapoptotic Bcl-2 family protein BAD. Mol Cell. 2004;13(3):329–40.

57. Li Z, Meng Z, Lu J, et al. TRPV6 protects ER stress-induced apoptosis via ATF6α-TRPV6-JNK pathway in human embryonic stem cell-derived cardiomyocytes. J Mol Cell Cardiol. 2018;120. https://doi.org/10.1016/j.yjmcc.2018.05.008.

58. Sun X, Sun G, Huang Y, et al. 3-Bromopyruvate regulates the status of glycolysis and BCNU sensitivity in human hepatocellular carcinoma cells. Biochem Pharmacol. 2020;177:113988. https://doi.org/10.1016/j.bcp.2020.113988.

59. Sun X, Fan T, Sun G, et al. 2-Deoxy-D-glucose increases the sensitivity of glioblastoma cells to BCNU through the regulation of glycolysis, ROS and ERS pathways: in vitro and in vivo validation. Biochem Pharmacol. 2022;199:115029. https://doi.org/10.1016/j.bcp.2022.115029.

Publisher's Note